Elementary Reaction Processes Involving Atomic and Molecular Oxygen on ZrB_2 (0001) Surface

P. Gamallo and R. Sayós *

Departament de Química Física and Institut de Química Teòrica i Computacional, Universitat de Barcelona, C. Martí i Franquès 1, 08028 Barcelona (Spain)

ABSTRACT

The interaction of atomic and molecular oxygen along with the atomic recombination on thin ZrB_2(0001) Zr- and B-terminated surfaces were studied using density functional theory (GGA/PBE) calculations. The adsorption of atomic oxygen is predominantly produced on threefold hollow sites for the Zr-finished surface and on B–B bridge sites for the B-finished surface. The experimental specular HREELS loss peaks and their shifts at high O exposures can be satisfactory explained by the present calculations. The interaction of O_2 over both terminated surfaces produces mainly its dissociation through non-activated processes. This fact is in agreement with the observed open dissociation at room temperature. The atomic oxygen recombination over both ZrB_2 surfaces shows that the Eley-Rideal reaction will be much more important than the Langmuir-Hinshelwood reaction at all temperatures and even more accessible in the case of the B-finished surface.

Keywords: Density functional theory, Eley-Rideal reaction, Langmuir-Hinshelwood reaction, atomic recombination, molecular dissociation

Tables: 6
Figures: 5
Proofs to: Dr. R. Sayós

(version: 15/2/2013)

I. INTRODUCTION

Zirconium diboride (ZrB_2) is member of a family of materials known as ultra high-temperature ceramics (UHTCs) [1-2], which are candidates for use in complex environments associated with hypersonic flights, atmospheric re-entry and rocket propulsion [3]. Due to the recent efforts in developing hypersonic aerospace vehicles as well as re-usable atmospheric re-entry vehicles [4], the attention to ZrB_2-based ceramics has increased appreciably in the last years (e.g., NASA-Ames Research Center [5]). These UHTCs could be used to increase the heat tolerance resistance of the thermal protection systems (TPSs) of these vehicles [6]. Their high melting points (i.e., ~ 3245 °C for pure ZrB_2), relatively low densities, good chemical stabilities (e.g., for erosion/corrosion), high hardness, high thermal stress resistance and high electrical and thermal conductivities [7] are perfect properties for such kind of applications.

Two important chemical processes concerning these ceramics involve atomic and molecular oxygen: 1) oxidation and 2) catalytic atomic recombination.

ZrB_2 undergoes stoichiometric oxidation when is exposed to air at elevated temperatures [7]:

$$ZrB_2(s) + \frac{5}{2}O_2(g) \rightarrow ZrO_2(s) + B_2O_3(l) \qquad \Delta G^0_{reac} = -1977 + 0.361T(°C) \ \ (kJ/mol) \quad (1)$$

although this process is favourable at all temperatures; only at temperatures below ~1100 °C, ZrO_2 and B_2O_3 form a continuous layer that produces a passive protection against oxidation. At higher temperatures (~1100-1400 °C) the change in weight arises from a combination of mass loss due to B_2O_3 evaporation and mass gain due to the formation of condensed oxides. The addition of other species over ZrB_2-based UHTCs (e.g., SiC [7], $TaSi_2$ [2],..) produces some improvements on their oxidation resistance. Nevertheless, the correlation between oxidation kinetics and oxygen transport mechanisms is not fully understood. On the other hand, an experimental study by high-resolution electron energy loss spectroscopy (HREELS) for O_2 adsorption on the ZrB_2 (0001) single crystal surface [8] demonstrates the molecular dissociative adsorption at room temperature, being the threefold hollow site suggested to be the most probable atomic adsorption site when the surface is Zr-finished and with a vibrational frequency in the range 491-557 cm^{-1}.

The apparently small heterogeneous atomic oxygen recombination over this kind of UHTCs can be very relevant for hypersonic flights through Earth's atmosphere [3]. N_2 and O_2 molecules dissociate at different extent in these extreme conditions (their D_o dissociation energies are 9.76 and 5.12 eV, respectively [9]). Thus, the more abundant atomic oxygen diffuses to the vehicle surface and recombines there (i.e., via Eley-Rideal or Langmuir-Hinshelwood mechanisms) transferring some fraction of its dissociation energy to the surface as heat. The control of this aerodynamic

heating by means of appropriate TPSs is essential for successful missions [4] in order to avoid tragedies as the Space Shuttle Columbia disintegration. In particular, very few experimental studies have been carried out about the O recombination over ZrB_2-based ceramics. Diffusion-tube side-arm reactor studies for a UHTC (ZrB_2 with 20-vol % SiC) [8] show a small but non-negligible atomic recombination coefficient (γ) that increases from 300 to 673 K, but decreases sharply (2 orders of magnitude) at 923 K. This behaviour was explained by the formation of a B_2O_3 surface oxide. Nevertheless, experimental measurements with a similar UHTC (ZrB_2 with 15-vol % SiC) at higher temperatures (1000-2000 K) and low pressure (200-400 Pa) air plasma [10-11] showed γ coefficients ranging from 0.01 at about 800 K to 0.1 at 1800 K, increasing with the augment of temperature, following an Arrhenius-type law with activation energy values of 0.25 and 0.29 eV for 200 and 400 Pa of total pressure, respectively. There was also observed some differences depending on the kind of surface mechanical treatment used for preparing the material.

The study presented here, is related with thin layers of ZrB_2, which presents similar surface energies for both Zr- and B-terminated surfaces with small relaxation. This situation gives us the opportunity of studying the reactivity on both kind of faces of zirconium diboride, which are also good substrates for adsorption due to the presence of several empty orbitals, *p* and *d* in boron and zirconium atoms, respectively.

This paper is organized as follows: a brief report of theoretical and computational aspects are described in Sec. 2, the results including bulk ZrB_2 properties and atomic and molecular oxygen adsorption processes along with atomic oxygen recombination reactions are presented in Sec. 3 and finally, Sec. 4 contains the main concluding remarks.

II. COMPUTATIONAL METHOD

Density Functional Theory (DFT) calculations have been performed with the VASP program [12,13,14,15] based on plane wave basis set. All the calculations reported here have been carried out at the spin-polarized generalized gradient correction (GGA) level of the density functional theory, using the Perdew-Burke-Ernzerhof functional (PBE) [16,17,18,19]. The atomic cores were described by projector augmented wave (PAW) pseudopotentials [20,21] allowing 3, 6 and 12 valence electrons for B, O and Zr atoms, respectively. The energy cut-off for the plane wave expansion was 550 eV, which produces well-converged results. Integration over the Brillouin zone was performed by using different k-points meshes (e.g., 5x5x1 and 14x14x14 for slab and bulk calculations, respectively) to ensure the total convergence of the results. The convergence criterion was 10^{-5} eV for the self-

consistent electronic minimization. Structural optimization was stopped when the x-, y- and z-components of the atomic forces were smaller than 0.02 eV/Å.

The transition states have been located with the nudged elastic band (NEB) method [22,23] using at least seven images between the reactant and the product structures. The structure of the highest energy structure found by the NEB algorithm was optimized and afterwards it was also characterized by a vibrational analysis computed with an energy accuracy of 10^{-6} eV.

In the adsorption studies we have used (1x1) and (2x2) surface unit cells for the ZrB_2 (0001) slab. A thin layer of the material (i.e., thickness between 5-6 Å) has been modelled using a 4 layer slab and taking into account the two possible terminations (Zr and B). The vacuum between slabs (17 Å) was large enough to prevent significant interactions between them. Several adsorption sites were studied for both O and O_2 species. In spite of some calculations were initially made fixing the spin magnetic moment for several states (e.g., singlet or triplet states for O_{ad}), we report the final spin-polarized structure which correspond to the most stable state.

Once determined the optimal geometry for each adsorption site (without any symmetry restriction), we also calculated the Hessian matrix and its corresponding harmonic vibrational frequencies (ν_i) for the adsorbed species (i.e., allowing to move only the O or O_2 species while keeping the slab atoms fixed to their positions in the equilibrium geometry). For an adatom these frequency values can be approximately classified as two parallel and one perpendicular movement, when the slab geometry is kept fixed to the optimized value. Moreover, some deeper vibrational analysis were carried out adding as well the first surface atoms not for focussing on the phonon analysis but to let us know how affect the outermost slab layer movement to the adsorbed atom's vibrational modes.

The adsorption energy (E_{ad}) per atom was defined as

$$E_{ad} = -\left(E_{atom+surf} - E_{surf} - n \cdot E_{atom}\right) / n \qquad (2)$$

where E_{atom} is the total ground state energy of the O atom in gas phase (i.e., O(^{3}P)), E_{surf} is the surface (clean slab) energy at its relaxed geometry for each possible termination, $E_{atom+surf}$ is the energy of the partial relaxed slab containing the adsorbed species and n indicates the number of atoms adsorbed on the surface. An analogous expression was used for molecular adsorption.

O and O_2 energies were calculated with the atom/molecule inside large broken symmetry boxes (i.e., 8 x 7.5 x 7.6 Å^3 and 10 x 10.5 x 10.6 Å^3, respectively). The well known DFT energy uncertainties (approximately 0.1-0.2 eV) [24] for atomic degenerate ground states (e.g., B or O atoms) should be considered not so relevant in this context where large adsorption energies are obtained. On the other hand, it is expected that these uncertainties will be lower or similar to the differences

in E_{ad} that can be derived by using other functionals, as it was established in similar studies that presented deviations in adsorption energy around 0.5 eV [25].

III. RESULTS AND DISCUSSION

BULK AND SLAB CALCULATIONS

A primitive rhombohedral (P6/mmm space group symmetry) unit cell with a single ZrB_2 formula unit can be used to describe the ZrB_2 bulk. The hexagonal cell results in a stacking of alternate layers of zirconium and boron atoms, each zirconium having 12 equidistant boron neighbours, six in the plane above and six in the plane below. The boron planes are equivalent to a graphite-like structure. As many transition metal diborides, ZrB_2 shows mixed bonding nature with a strong covalent bonding between B, metallic between Zr, and ionic and covalent between Zr and B [26, 27].

We have calculated the main bulk properties to verify the reliability of the present DFT approach to reproduce ZrB_2 surface. We have carried out a complete minimization of both the force acting over each atom and the stress tensor allowing volume and shape relaxation in order to obtain the equilibrium lattice parameters. Table I presents these lattice parameters (a=b, c) together with the cohesive energy (E_{coh}), the heat of formation ($\Delta_f H_{o\ K}$), the bulk modulus (B_o) and its pressure derivative (B_o') for ZrB_2 compound along with some comparison with earlier DFT studies and with available experimental data. B_o and B_o' were derived by using a third-order Birch-Murnaghan state equation. The calculated structural properties compare very well with both experimental data and previous theoretical studies.

Experimental studies by means of coaxial impact-collision ion scattering spectroscopy [32] and surface phonon-dispersion data measured by HREELS [33] corroborate that the ZrB_2(0001) surface is terminated with a Zr layer. This conclusion is supported by several DFT studies [34,35] that show that the Zr-terminated surface is more stable than the B-terminated over a wide range of allowed chemical potentials. Nevertheless, the slab thickness is very important in the stability of the structure. Thus, for thin films of ZrB_2 the corresponding surface energy for both types of terminations are very similar and even in certain cases (i.e., thickness tends to zero) the B-termination is the preferred one [34, 35]. According to this, surface calculations have been done by using slabs with a different number of layers (i.e., thickness) for both Zr- and B-terminations and starting always from the calculated bulk geometry. Symmetric (5 or 11 layers corresponding to a thickness of 7 or 18 Å, respectively) or stoichiometric (4 or 10 layers corresponding to a thickness

of 5.5 or 16.5 Å, respectively) slabs were considered. Obviously, the vacuum used within these models has been appropriately maintained within the range 17 - 18 Å for avoiding non-desirable interactions between the slabs. Regarding to the different slab models used, the symmetric ones should reduce the spurious dipole effects while the stoichiometric ones would evidently represent better the correct ZrB_2 stoichiometry. Table II shows the calculated interlayer relaxations (i.e., Δd_{ij}) for Zr- and B-terminated surfaces. The most significant feature is the noteworthy inward relaxation of the surface plane for both terminations (larger in the case of B-terminated surface) together with a much less outward relaxation of the inner layers. These results are in good agreement with previous theoretical data [35, 36], which show that these relaxations affect mainly the first three layers for the Zr-terminated surface and the outermost four-five layers in the B-terminated case. Moreover, no significant differences arise in comparing symmetric vs. stoichiometric slab models (c.f., 10 vs. 11 layer slab results). On the other hand, the slab models with 4 or 5 layers seem to be accurate enough for atom/molecule adsorption calculations.

OXYGEN ADSORPTION

We have studied the adsorption of atomic oxygen on seven different sites over the unit cell of ZrB_2 (0001) surface finished in Zr or B layers (Fig. 1). For the Zr-terminated surface (Fig. 1b), there is a hollow site (H1) in which the adatom coordinates three Zr atoms of the same layer; the other two explored sites are a bridge site (B1) between two Zr atoms and a Zr top site (T1). In the case of the B-terminated surface (Fig. 1c), there are 4 relevant sites: a bridge between two B atoms (B2), a six-fold hollow site (H2) in the centre of the B hexagon, a B top site (T2) and a site located in the middle between H2 and B2 sites (M2).

Table III summarizes the results for the atomic oxygen adsorption over the seven sites listed above for a four-layer slab model, where the two first layers were allowed to relax. These values were obtained keeping free the spin polarization although very similar results were also taken fixing the spin state during the oxygen adsorption (i.e., singlet and triplet). From the values obtained, a different behaviour is patent for the two kinds of surfaces. In the case of the Zr-termination, the most stable site is the H1 one (E_{ad} = 8.53 eV), decreasing the adsorption energy in the order H1 > B1 > T1. However only the H1 stationary point corresponds to a true minimum with all positive vibrational frequencies. The calculated O-Zr distance for this adsorption minimum is quite close to the expected values in a typical crystalline solid as zirconia (2.221 Å and 2.141 Å for cubic [37] or orthorhombic [38] structures, respectively). The three Zr atoms in the H1 site are almost not shifted by the O adsorption in comparison with other Zr atoms of the same first layer.

Moreover, we have also checked the description of the minimum adsorption site (i.e., H1) by using a five-layer slab model (which describes slightly better the clean slab). The resulting structure is almost the same reported in Table III (e.g., E_{ad} = 8.51 eV, d(O-Zr) = 2.133 Å and d(O-B) = 2.989 Å). It is also important to note that this H1 site, which corresponds to the most stable threefold hollow site predicted by the present study, is in complete agreement with HREELS experimental predictions [8].

The other sites B1 and T1 correspond to first- and second-order saddle points, respectively, and they are associated with diffusion over the surface. Thus, B1 is a diffusion transition state that connects two adjacent H1 minima (i.e., H1 $\rightarrow$ B1$^{\neq}$ $\rightarrow$ H1) with an energy barrier of 0.57 eV. When the adatom is on T1 site, two different diffusion paths are available since the site is surrounded by six B1 and six H1 sites (Fig. 1b). Hence, the connection can involve two opposite H1 minima (H1 $\rightarrow$ T1$^{\neq}$ $\rightarrow$ H1) or two B1 sites (B1$^{\neq}$ $\rightarrow$ T1$^{\neq}$ $\rightarrow$ B1$^{\neq}$), with much larger energy barriers (2.65 eV and 2.08 eV, respectively).

In the case of boron termination, the most stable site is a bridge between two neighbouring boron atoms (B2, E_{ad} = 6.30 eV) whereas the other three possible sites are stationary points related with the diffusion among the different surface sites, decreasing their adsorption energy in the order B2 > M2 > T2 > H2. The calculated B-O distances for the most stable site (B2) are similar to those observed experimentally in borates or boric acids (e.g., 1.367-1.371 Å in H_3BO_3 [39] or 1.363-1.561 Å HBO_2 [40]). Diffusion between two adjacent B2 minima can occur through a high-energy barrier of 1.02 eV (B2 $\rightarrow$ M2$^{\neq}$ $\rightarrow$ B2). Moreover, M2 sites surrounding the same B atom are connected through T2 (M2$^{\neq}$ $\rightarrow$ T2$^{\neq}$ $\rightarrow$ M2$^{\neq}$) whereas M2 of different B atoms can be connected through H2 transition state (M2$^{\neq}$ $\rightarrow$ H2$^{\neq}$ $\rightarrow$ M2$^{\neq}$), with very different energy barriers (0.31 eV and 2.32 eV, respectively).

The atomic coverage effect has also been studied, considering a two O atom adsorption in the same (2x2) supercell, which means an increase from 12.5 to 25 % of coverage taking into account only the H1 minimum sites for the Zr-terminated face or from 8.3 to 16.7% for considering only the B2 minimum sites for the B-terminated surface. When an initial oxygen atom is preadsorbed on a first H1 hollow site, a second O can be adsorbed on one of the three non-equivalent H1 sites (labelled as H1(A), H1(B) and H1(C)) as it is indicated in Fig. 2a and Table IV. The adsorption energy per atom is larger when both H1 sites are as far as possible (i.e., H1 + H1(C)), arising then similar adsorption energy and geometry as for a single atom adsorption. A clear shift in vibrational frequencies is also observed. For instance, perpendicular frequencies increase not only with atomic

coverage but also and in a greater extent when the adatoms are in nearer H1 sites (i.e., at lower O-O distances).

In the case of the B terminated surface there are four non-equivalent B2 sites for the second O atom (Fig. 2b) although we observe only small differences respect their adsorption energies and geometries (Table IV). In principle, a similar trend in E_{ad} values could be expected as for Zr-termination, explaining the similar stability for two-atom adsorption in B2 + B2(D) in comparison with one-atom adsorption on B2 site, where O-O distance is large enough (3.179 Å) and no interaction between O atoms is expected as in the single atom adsorption case. In this latter configuration both O adatoms are in different B hexagons but when those oxygen atoms are in the same hexagon the behaviour seem to be rather different and their stability decreases (e.g., in B2 + B2 (C)) respect one single atom adsorption. Moreover a larger E_{ad} is observed for shorter O-O distances (i.e., B2 + B2(A) > B2 + B2(B) > B2 + B2(C)). This can be explained in terms of the important surface (slab) reconstruction (e.g., Δz = 0.986 Å for B2 + B2(A)) produced in the first boron layer (Fig. 3), which gives an E_{ad} even greater than for the case of a single atom adsorption. Thus, the B-O distances become shorter (Table IV) and both <BOB angles become larger (i.e., (88.6 °, 88.69 °), (86.0 °, 111.5 °) and (113.1 °, 113.1 °) for C, B and A cases, respectively), approaching the experimental B-O distances and <BOB angles observed in H_3BO_3 [39] or in HBO_2 [40] crystalline structures (i.e., <BOB angles within 118-121º and 119-120º intervals, respectively).

The specular HREELS spectra for oxygen-exposed ZrB_2 (0001) surfaces [8] show a loss peak at 60.9 meV (491.2 ± 16 cm^{-1}). When atomic exposure increases this peak shifts towards a higher energy of 69.1 meV (557.3 ± 16 cm^{-1}) increasing also its intensity. As this technique detects mainly the dipole-active modes (i.e., only the perpendicular modes which change the dynamic dipole moment) the peak is in agreement with present DFT results for the adsorption of one oxygen atom on H1 site (Table III) that show a perpendicular active mode at 462.8 cm^{-1} for the lowest coverage. The inclusion of the Zr atoms of the first layer into the vibrational frequency analysis produces an increase of 4-5% (i.e., 488.4 cm^{-1}, 361.4 and 360.4 cm^{-1}), in even better agreement with the experimental data. For slightly higher coverages (i.e., 25% corresponding to the adsorption of two O atoms) the DFT results (Table IV) show a shift of the active mode to 454.3, 481.7 or 663.1 cm^{-1} depending on the closeness of both H1 occupied sites (H1 + H1(C), H1(B), H1(A), respectively). It is worth noting that only one of the two perpendicular modes listed in Table IV (the symmetric one) is active. At this 25% of coverage the most favourable adsorption would be mainly produced in H1 + H1(B) or H1 + H1(C) pair of sites that keep the two O-O atoms still far from each other,

which would produce a peak within the 56.3-59.7 meV range, justifying thus the experimental 60.9 meV peak.

A further increase in the coverage produces an increment of the vibrational frequency of this perpendicular active mode, which can justify clearly the shift of the experimental peak from 60.9 to 69.1 meV. Thus, DFT calculations for 3 (37.5% of coverage) or 4 (50% of coverage) oxygen atoms adsorbed in the same type of hollow sites (i.e., all upward or all downward) within the (2x2) supercell produce values of 492.0 and 511.5 cm^{-1}, respectively, which also correspond to adsorption energies per atom of 8.14 and 7.92 eV, respectively, only slightly less stable in comparison with lower coverage values (Tables III and IV). The inclusion of more O atoms decreases largely the adsorption energy per atom (e.g., 6.49, 5.96, 5.33 and 3.90 eV for 6, 7, 8 or 8 atoms, respectively), possibly because these additional O atoms occupy now nearest neighbour sites with a stronger but unfavourable O-O interaction. This behaviour was also predicted for H adsorption on the same surface [41], which shows as well that the most stable coverage is around 50%, being this value close to the saturation coverage one. At very high oxygen exposures the observed streaky LEED patterns [8] confirm these strong O-O interactions.

On the other hand, at high O exposures two small additional experimental loss peaks were also detected at 52-53 meV (419.4-427.5 ± 16 cm^{-1}) and 87.7 meV (707.3 ± 16 cm^{-1}) [8]. Possible explanations based on the presence of some peroxo species (e.g., O_2^{2-}) or in some subsurface oxygen caused by some vacancies were proposed for the larger loss peak. Some Zr vacancies would put the B-layer more accessible for the incoming O atoms. In addition, the large outward relaxation observed for O adsorption in the outermost boron layer for a B-finished surface (e,g., in B2 + B2(A), Fig. 3b) could justify the penetration and adsorption of O over the accessible boron subsurface layer at these coverages. This fact can be reinforced not only for the similar surface energies observed for both slab terminations in thin ZrB_2 layers [35] but also by the large adsorption energy calculated for B2 sites. Therefore, this peak at 87.7 meV could be also produced by O-B stretching modes, whose calculated vibrational frequencies for B2 sites (i.e., 706.1 cm^{-1} (Table III) or 725.6-891.5 cm^{-1} (Table IV) for 8.3 % and 16.7 % coverages, respectively) are very close to the experimental value (707.3 ± 16 cm^{-1}). However, another possible explanation could come from the fact that at higher coverage the top Zr sites (T1) become more available and their calculated associated frequencies (i.e., 700.1 cm^{-1}, Table III) would be also compatible with the loss peak of 87.7 meV. At lower coverage only the most stable H1 sites would be occupied justifying the absence of this peak.

We have also studied the molecular interaction of oxygen on ZrB_2 (0001) for both terminated surfaces. Molecular oxygen can only be adsorbed dissociatively (not molecularly) over the Zr-terminated surface, which is a non-activated process (i.e., without any energy barrier) with both O final adatoms occupying two consecutive threefold hollow sites (i.e., H1 + H1(A), Fig. 2a), in good agreement with the experimental open dissociation at room temperature for both O_2 and H_2 molecules [8]. Moreover, similar DFT results were reported for H_2 dissociation on the same surface [41]. However, the B-terminated surface presents a somewhat different behaviour as shown in Figure 4. Thus, when O_2 approach parallel to the surface there is a non-activated molecular adsorption with an adsorption energy of 2.63 eV respect O_2 gas (MIN1 in Table V). From this minimum there is a small energy barrier of 0.27 eV (zero point energy not included) corresponding to a transition state (TS2 in Table V) which dissociates to B2 + B2(B) sites. The parallel asymmetric imaginary frequency allows the movement of both oxygen atoms in opposite way until reaching two non-consecutive B2 sites. However, for a perpendicular molecular approach there is a small energy barrier of 0.39 eV (zero point energy not included), corresponding to another transition state (TS1 in Table V) connecting also with the molecular minimum (MIN1, Fig. 4).

Materials with a low oxidation rate are required for hypersonic applications whereas the present DFT calculations confirm the great capability of both ZrB_2 surfaces to be oxidized by either molecular or atomic oxygen. This fact justifies accordingly the necessity of adding other species on ZrB_2-based UHTCs in order to increase their oxidation resistance (e.g., SiC [7], $TaSi_2$ [2],..).

ATOMIC OXYGEN RECOMBINATION REACTION

We have also studied the atomic oxygen recombination over the ZrB_2 surface with the two possible surface terminations through two typical mechanisms: Eley-Rideal (ER: $O_{(g)} + O_{(ad)}$) and Langmuir-Hinshelwood (LH: $O_{(ad)} + O_{(ad)}$). As the preadsorbed oxygen prefers the most stable adsorption sites, this study was focused on considering one or two O adsorbed on H1 and B2 sites for Zr- and B-terminated surfaces, respectively. A first analysis on their exo- or endothermicities (ΔE_{reac}) reveals that the ER reaction will be much more accessible than LH reaction at all temperatures or collision energies because ΔE_{reac} (zero point energy not included) for ER is much lower than for LH (2.49 and 9.62 eV for Zr-terminated surface and 0.26 and 6.21 eV for B-terminated surface, respectively). The minimum energy path for ER reaction over the Zr-terminated surface has not shown any additional transition state; thus, its energy barrier corresponds only to the whole endothermicity.

A different scenario is observed in the case of the B-terminated surface. When the incoming oxygen gas atom approaches to the adatom preadsorbed on B2 site, a new minimum structure (MIN2, Table VI) is formed without an energy barrier, adopting both O atoms a perpendicular configuration respect to the surface (Fig. 5). From this minimum is possible to produce directly $O_{2(g)}$ surpassing a second-order transition state (TS3, Table VI) through the perpendicular imaginary frequency (ν = 137.2i cm^{-1}), which also can reach the most stable molecular adsorption minimum (MIN1) following through the another imaginary frequency (ν = 285.4i cm^{-1}) that describes mainly a parallel movement although with some perpendicular character.

According to these facts, the ER reaction will be much more important than LH reaction in both terminated ZrB_2 surfaces, although the ER reaction would be more available for the B-finished surface (0.26 eV of endothermicity and 0.51 eV of energy barrier). However, the Zr-terminated surface results should be more relevant in comparison with the experimental data of the catalytic efficiency for the recombination of atomic oxygen on ZrB_2-based ceramics. In spite of the addition of SiC (15-vol %) to ZrB_2 can alter its reactivity, the experimental activation energies (0.25 and 0.29 eV for 200 and 400 Pa of total pressure, respectively [11]) are very close to the present DFT results for a low coverage limit. However, the inclusion of SiC compound and the effect of the high experimental temperatures (800-1800 K) should be introduced in additional theoretical calculations (i.e., kinetic and dynamics studies) to make a more reliable comparison.

IV. SUMMARY AND CONCLUDING REMARKS

Density functional theory (GGA/PBE) calculations were carried out to describe the main ZrB_2 bulk properties together with the interaction of atomic and molecular oxygen with thin films of zirconium diboride, considering both Zr- and B-terminated (0001) surfaces. All the calculated structural properties (e.g., lattice parameters, cohesive energy, heat of formation, bulk modulus,…) compare satisfactorily well with either experimental data or earlier theoretical studies. Surface calculations using slabs with a different number of layers show a clear trend to inward relaxation of the surface plane for both terminations along with much less outward relaxations of the inner layers.

The adsorption of atomic oxygen is mostly favourable on threefold hollow sites (H1) for the Zr-finished surface and on B–B bridge sites (B2) for the B-finished surface. The calculated large stability on these H1 sites is in complete agreement with specular HREELS experimental predictions. The coverage effect has been studied showing a noticeable influence for the Zr-

terminated surface. The adsorption energy per atom is larger when both H1 sites are as far as possible. A clear shift in the perpendicular vibrational frequencies is observed when the coverage is augmented (462.8 → 492.0 → 511.5 cm^{-1}), which can explain the experimental loss peak shift from 491.2 to 557.3 ± 16 cm^{-1}. The most stable coverage was found around 50%, being this value close to the saturation one and similar to the previously calculated for the H adsorption over the same Zr-terminated surface.

Moreover, the additional experimental small peak observed at 707.3 ± 16 cm^{-1} for high O exposures could be explained considering an O-B stretching, which presents vibrational frequencies for B2 site (706.1 cm^{-1} or 725.6-891.5 cm^{-1} for 8.3 and 16.7% coverages, respectively) very close to the experimental value. However, another possible explanation could come from the O adsorption on top Zr sites at higher coverage.

The molecular interaction of oxygen over both terminated surfaces produce mainly its dissociation through non-activated processes, which is in agreement with the observed open dissociation at room temperature. Furthermore, O_2 can be molecularly adsorbed on the B-terminated surface adopting a more stable parallel configuration (E_{ad} = 2.63 eV).

The study of the atomic oxygen recombination over both ZrB_2 surfaces shows that the Eley-Rideal reaction will be much more important than the Langmuir-Hinshelwood reaction at all temperatures or collision energies. The ER reaction will be more accessible for the B-finished surface (only 0.26 eV of endothermicity and 0.51 eV of energy barrier), but it is less stable than the Zr-terminated one with a higher endothermicity. The DFT results for a low coverage limit are compatible with the experimental activation energies (i.e., 0.25-0.29 eV) derived for ZrB_2-based ceramics with 15-vol % SiC at high temperatures (800-1800 K), although additional theoretical calculations (i.e., kinetic and dynamics studies at high temperatures) including SiC into the slab should be necessary to make a more trustworthy comparison.

AUTHOR INFORMATION

Corresponding Author

***** Phone: +34 934034760. E-mail: r.sayos@ub.edu.

Notes

The authors declare no competing financial interest.

ACKNOWLEDGEMENTS

This work was supported in part by the Spanish Ministry of Science and Innovation (Project CTQ2009-07647) and by the Autonomous Government of Catalonia (Project 2009SGR1041).

REFERENCES

(1) Opeka, M.M.; Talmy, I.G.; Zaykoski, J.A. Oxidation-Based Materials Selection for 2000 °C + Hypersonic Aerosurfaces: Theoretical Considerations and Historical Experience. *J. Matt. Sci.* **2004**, 39, 5887-5904.

(2) Opila, E.; Levine, S.; Lorincz, J. Oxidation of ZrB_2- and HfB_2-Based Ultra-High Temperature Ceramics: Effect of Ta Additions. *J. Matt. Sci.* **2004**, 39, 5969-5977.

(3) Capitelli M. (ed.), *Molecular Physics and Hypersonic Flows*, *NATO ASI Series C, vol. 482*, Kluwer Academic Publishers: Dordrecht, 1996.

(4) Bertin, J.J.; Cummings R.M. Critical Hypersonic Aerothermodynamic Phenomena. *Annu. Rev. Fluid. Mech.* **2006**, 38, 129-157.

(5) http://www.nasa.gov/centers/ames

(6) Kovalev, V.L.; Kolesnikov A.F. Experimental and Theoretical Simulations of Heterogeneous Catalysis in Aerothermochemistry. *Fluid. Dyn.* **2005**, 40, 669-693.

(7) Fahrenholtz W.G.; Hilmas G.E.; Talmy I.G.; Zaykoski, J.A. Refractory Diborides of Zirconium and Hafnium. *J. Am. Ceram. Soc.* **2007**, 90, 1347-1364.

(8) Aizawa, T.; Hayami, W; Otani, S. Adsorption of H_2, $^2H_2$, O_2, and CO on ZrB_2 (0001). *J. Chem. Phys.* **2002**, 117, 11310-11314.

(9) Huber, K.P.; Herzberg, G. *Molecular Spectra and Molecular Structure*. *Vol*. *IV*. *Constants of Diatomic Molecules;* Van Nostrand Reinhold: New York, 1979.

(10) Marschall J.; Chamberlain, A.; Crunkleton D.; Rogers, B. Catalytic Atom Recombination on ZrB_2/SiC and HfB_2/SiC Ultrahigh-Temperature Ceramic Composites. *J. Space. Rock.* **2004**, 41, 576-581.

(11) Scatteia, L.; Alfano, D.; Monteverde F.; Sans, J-L; Balat-Pichelin, M. Effect of the Matching Method on the Catalycity and Emissivity of ZrB_2 and ZrB_2-HfB_2-Based Ceramics. *J. Am. Ceram. Soc.* **2008**, 91, 1461-1468.

(12) Kresse G.; Hafner J. Ab Initio Molecular Dynamics for Liquid Metals. *Phys. Rev. B* **1993**, 47, 558-561.

(13) Kresse G.; Hafner J. Ab Initio Molecular-Dynamics Simulation of the Liquid-Metal–Amorphous-Semiconductor Transition in Germanium. *Phys. Rev. B* **1994**, 49, 14251-14269.

(14) Kresse G.; Furthmüller J. Efficiency of Ab-initio Total Energy Calculations for Metals and Semiconductors Using a Plane-Wave Basis Set. *Comput. Mater. Sci.* **1996**, 6, 15-50.

(15) Kresse G.; Furthmüller J. Efficient Iterative Schemes for Ab Initio Total-Energy Calculations Using a Plane-Wave Basis Set. *Phys. Rev. B* **1996**, 54, 11169-11186.

(16) Perdew J.P.; Chevary J.A.; Vosko S.H.; Jackson K.A.; Pederson M.R.; Singh D.J.; Fiolhais C. Atoms, Molecules, Solids, and Surfaces: Applications of the Generalized Gradient Approximation for Exchange and Correlation. *Phys. Rev. B.* **1992**, 46, 6671-6687.

(17) Perdew J.P.; Chevary J.A.; Vosko S.H.; Jackson K.A.; Pederson M.R.; Singh D.J.; Fiolhais C. Erratum: Atoms, Molecules, Solids, and Surfaces: Applications of the Generalized Gradient Approximation for Exchange and Correlation. *Phys. Rev. B.* **1993**, 48, 4978-4978.

(18) Perdew J.P.; Burke K.; Wang Y. Generalized Gradient Approximation for the Exchange-Correlation Hole of a Many-Electron System. *Phys. Rev. B* **1996**, 54, 16533-16539.

(19) Perdew J.P.; Burke K.; Wang Y. Erratum: Generalized Gradient Approximation for the Exchange-Correlation Hole of a Many-Electron System. *Phys. Rev. B* **1998**, 57, 14999-14999.

(20) Kresse G.; Joubert J. From Ultrasoft Pseudopotentials to the Projector Augmented-Wave Method. *Phys. Rev. B* **1999**, 59, 1758-1775.

(21) Blöchl P.E. Projector Augmented-Wave Method. *Phys. Rev. B*. **1994**, 50, 17953-17979.

(22) Mills, G.; Jónsson H.; Schenter G.K. Reversible Work Transition State Theory: Application to Dissociative Adsorption of Hydrogen. *Surf. Sci.* **1995**, 324, 305-337.

(23) Henkelman G.; Jóhannesson G.; Jónsson H. : *Methods for finding saddle points and minimum energy paths*, in Theoretical Methods in Condensed Phase Chemistry, Schwartz S.D., Ed.; Kluwer Academic Publishers: the Netherlands, **2000**; Chapter 10, pp 269-302.

(24) Baerends E.J.; Branchadell V.; Sodupe M. Atomic Reference Energies for Density Functional Calculations. *Chem. Phys. Lett.* **1997**, 265, 481-489.

(25) Hammer B.; Hansen L.B.; Nørskov J.K. Improved Adsorption Energetics within Density-Functional Theory Using Revised Perdew-Burke-Ernzerhof Functionals. *Phys. Rev. B* **1999**, 59, 7413-7421.

(26) Vajeeston P.; Ravindran P.; Ravi C.; Asokamani R. Electronic Structure, Bonding, and Ground-State Properties of AlB_2-Type Transition-Metal Diborides. *Phys. Rev. B* **2001**, 63, 045115-1-12.

(27) Zhang X.; Luo X.; Han J.; Li J.; Han W. Electronic Structure, Elasticity and Hardness of Diborides of Zirconium and Hafnium: First Principles Calculations. *Compt. Mat. Sci.* **2008**, 44, 411-421.

(28) Eisenmann, B.; Schäfer, H. 3.2 References for 3.1. Hellwege, K.H.; Hellwege, A.M.(ed). SpringerMaterials-The Landolt-Börnstein Database (http:/www.springermaterials.com)

(29) Chase Jr. M.W., NIST-JANAF Themochemical Table, *J. Phys. Chem. Ref. Data* **1998**, Monograph 9, 1-1951.

(30) Okamoto N.L.; Kusakari M.; Tanaka K.; Inui H.; Yamaguchi M.; Otani S. Temperature Dependence of Thermal Expansion and Elastic Constants of Single Crystals of ZrB_2 and the Suitability of ZrB_2 as a Substrate for GaN Film. *J. Appl. Phys.* **2003**, 93, 88-93.

(31) Pereira A.S.; Perottoni C.A.; da Jornada J.A.H.; Léger J.M.; Haines J. Compressibility of AlB_2-Type Transition Metal Diborides. *J. Phys. Condens. Matter* **2002**, 14, 10615-10618.

(32) Suto H.; Fujii S.; Miyamae N.; Armitage R.D.; Suda J.; Kimoto T.; Honda S.; Katayama M. Structure Analysis of ZrB_2 (0001) Surface Prepared by ex situ HF Treatment. *Jpn. J. Appl. Phys.* **2006**, 45, L497-L500.

(33) Aizawa T.; Hayami W; Otani S. Surface Phonon Dispersion of ZrB_2(0001) and NbB_2(0001). *Phys. Rev. B* **2001**, 65, 024303-1-9.

(34) Liu P.L.; Chizmeshya A.V.G.; Kouvetakis, J.; Tsong I.S.T. First-Principles Studies of GaN (0001) Heteroepitaxy on ZrB_2 (0001). *Phys. Rev. B* **2005**, 72, 245335-1-7.

(35) Zhang X.; Luo X.; Li J.; Han J.; Han W.; Hong C. Structure and Bonding Features of ZrB_2 (0001) Surface. *Compt. Mat. Sci* **2009**, 46, 1-6.

(36) Aizawa T.; Suehara S.; Hishita S.; Otani S.; Arai, M. Surface Core-Level Shift and Electronic Structure on Transition-Metal Diboride (0001) Surfaces. *Phys. Rev. B* **2005**, 71, 165405-1-9.

(37) Martin U.; Boysen H.; Frey F. Neutron Powder Investigation of Tetragonal and Cubic Stabilized Zirconia, TZP and CSZ, at Temperatures up to 1400 K. *Acta Cryst. B* **1993**, 49, 403-413.

(38) Kisi E. H.; Howard, C. J.; Hill, R. J. Crystal Structure of Orthorhombic Zirconia in Partially Stabilized Zirconia. *J. Amer. Cer. Soc.* **1989**, 72, 1757-1760.

(39) Gajhede M.; Larsen S.; Rettrup S. Electron Density of Orthoboric Acid Determined by X-Ray Diffraction at 105 K and Ab Initio Calculations. *Acta. Cryst. B* **1986**, 42, 545-552.

(40) Freyhardt, C. C.; Wiebcke, M.; Felsche, J. The Monoclinic and Cubic Phases of Metaboric Acid (Precise Redeterminations). *Acta. Cryst. C* **2000,** 56, 276-278.

(41) Walkosz W.; Manandhar K.; Trenary M.; Otani S.; Zapol P. Dissociative Adsorption of Hydrogen on the ZrB_2(0001) Surface. *Surf. Sci.* **2012,** 606, 1808-1814.

FIGURE CAPTIONS

Figure 1. Side (a) and top views (b, c) of the ZrB_2 (0001) slab model with a Zr (a, b) and a B (c) topmost layer , respectively. The different adsorption sites are shown for each termination. Red line defines the (2x2) supercell. Blue and green circles stand for Zr and B atoms, respectively.

Figure 2. Non-equivalent minimum adsorption sites available for a second O atom when a first one is previously adsorbed on H1 (Zr-terminated slab) or B2 (B-terminated slab) sites in a (2x2) supercell. Blue, green and red circles stand for Zr, B and O atoms, respectively.

Figure 3. Top (top panels) and side (bottom panels) views of a) clean slab and two-atom adsorption cases on the B-terminated surface: b) B2 + B2(A), c) B2 + B2(B), d) B2 + B2(C) and e) B2 + B2(D). In the bottom panels the last boron layer was kept fixed in the optimization process while the other layers were allowed to relax. Blue, green and red circles stand for Zr, B and O atoms, respectively. For clarity, the atoms belonging to the two lowest layers are drawn translucent in order to focus the attention on the outermost boron layer.

Figure 4. Minimum energy path for the molecular adsorption over the B-terminated surface. Insets point out the stationary points listed in Tables VI and V. Green and red circles stand for B and O atoms, respectively.

Figure 5. Minimum energy path for the ER atomic oxygen recombination reaction on B-terminated surface. Insets point out the stationary points listed in Table V. Green and red circles stand for B and O atoms, respectively.

Fig. 1

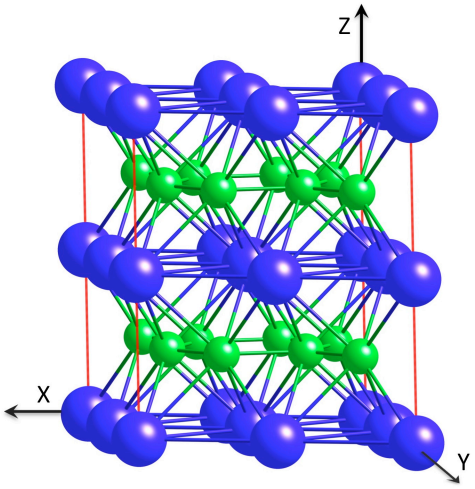

(a)

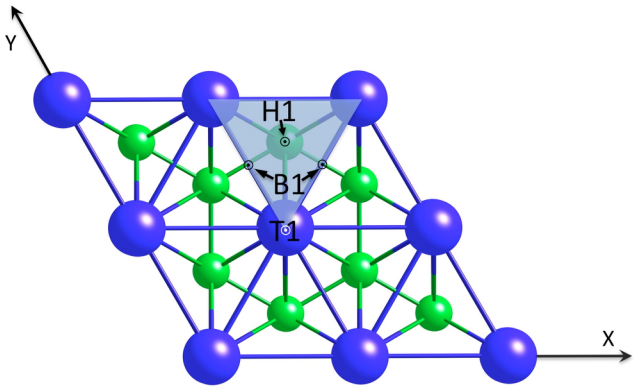

(b)

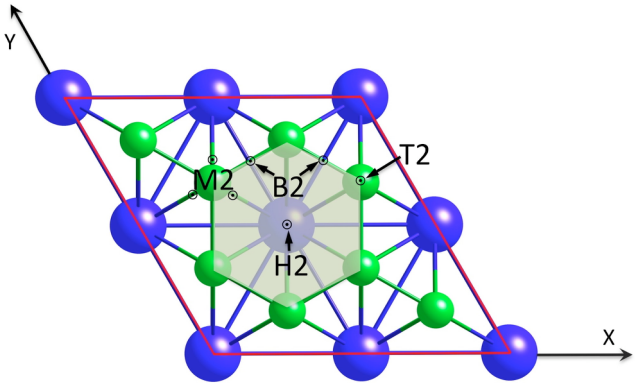

(c)

Fig. 2

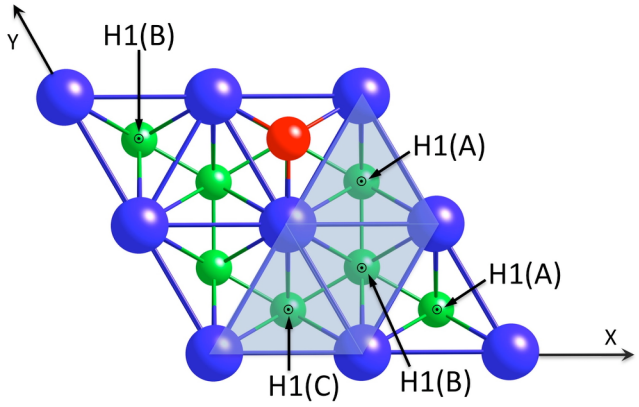

(a)

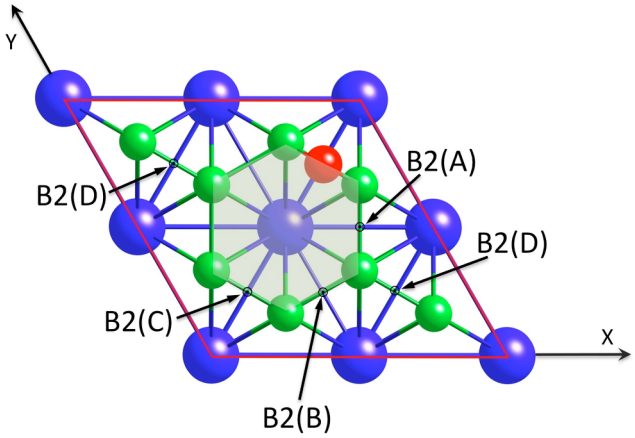

(b)

Fig. 3

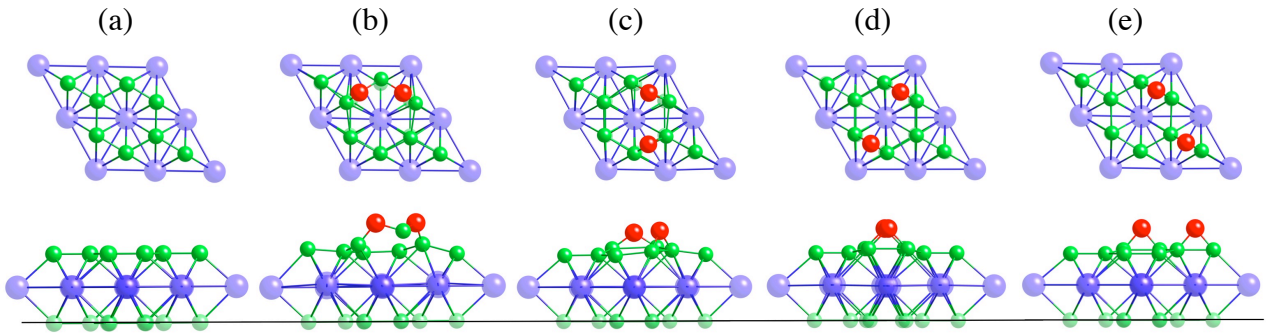

Fig. 4

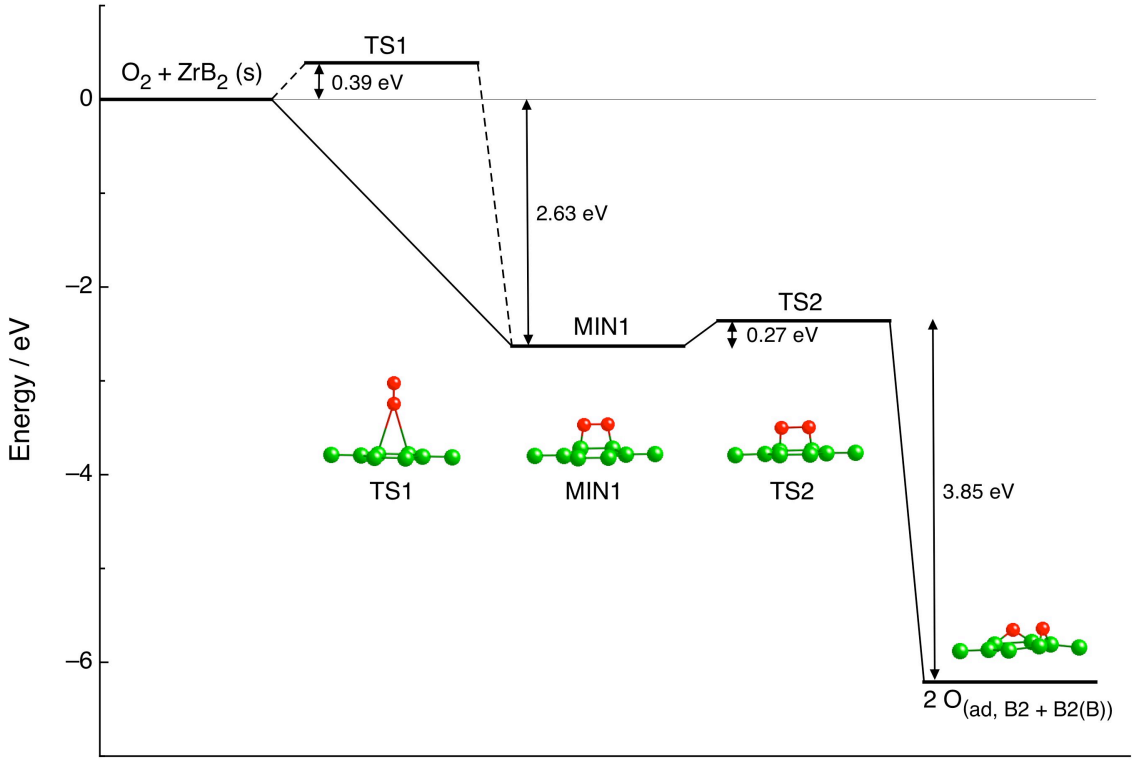
TS1
$O_2 + ZrB_2$ (s)
0.39 eV
0
2.63 eV
−2
MIN1
TS2
0.27 eV
Energy / eV
−4
TS1
MIN1
TS2
3.85 eV
−6
2 $O_{(ad, B2 + B2(B))}$

Fig. 5

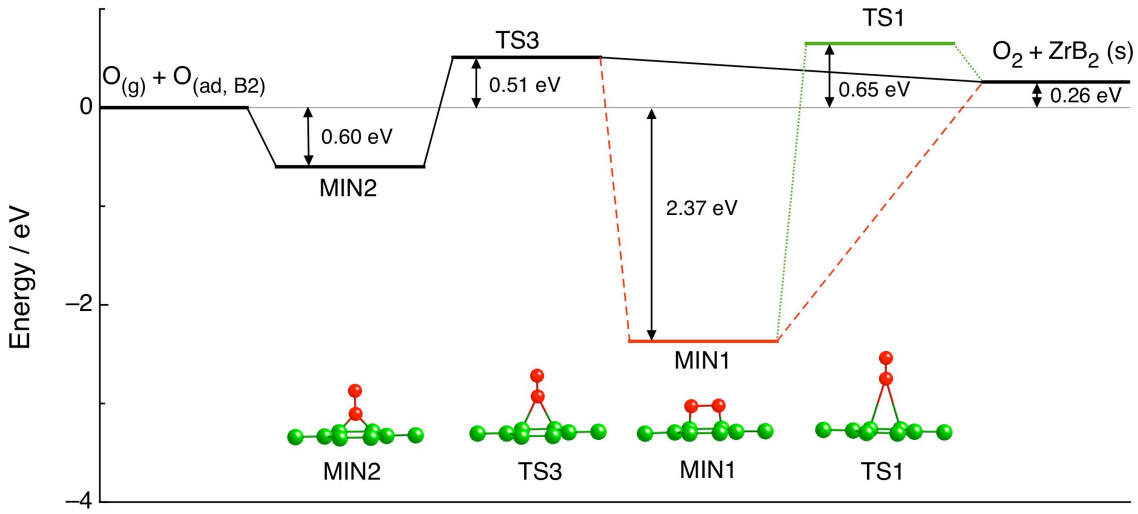
TS1
TS3
$O_2 + ZrB_2$ (s)
$O_{(g)} + O_{(ad, B2)}$
0.51 eV
0.65 eV
0.26 eV
0
0.60 eV
MIN2
2.37 eV
Energy / eV
−2
MIN1
−4
MIN2
TS3
MIN1
TS1

TOC (Table of Contents)

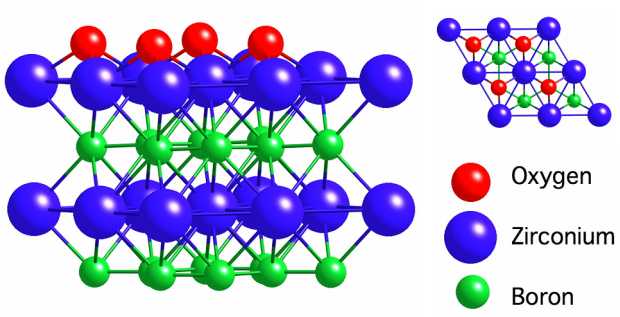

TABLE I. Calculated and experimental lattice parameters, equilibrium volume, interatomic distances, cohesive energy, heat of formation, bulk modulus and its pressure derivative of ZrB_2 compound

Method	a (Å)	c (Å)	V_o (Å^3/cell)	d_{Zr-B} (Å)	d_{B-B} (Å)	E_{coh} (eV/cell)	$\Delta_f H_{o\,K}$ (eV/cell)	B_o (GPa)	B_o'
GGA-PBE (PAW) [a]	3.179	3.554	31.105	2.554	1.835	21.68	-2.971	244	3.89
TB-LMTO-ASA [b]	3.197	3.561	31.520	2.565	1.846	17.01	-3.076	195	1.94
GGA-PBE (USP) [c]	3.168	3.536	30.731	2.544	1.829	23.911	-3.055	238	3.84
Experiment	3.169 [d]	3.531 [d]	30.710	2.543	1.830	21.14±0.40 [e]	-3.33±0.07 [e]	245 [f], 317 [g]	-

[a] This work. B_o and B_o' are derived from third-order Birch-Murnaghan state equation; $\Delta_f H$ is calculated from $\Delta_f H^{ZrB_2} = E^{ZrB_2}_{bulk(eq.)} - \left[E^{Zr}_{bulk(eq.)} + 2E^{B}_{bulk(eq.)}\right]$ and E_{coh} from $E^{ZrB_2}_{coh} = \left[E^{Zr}_{atom} + 2E^{B}_{atom}\right] - E^{ZrB_2}_{bulk(eq.)}$

[b] Theoretical data from Ref. 26.

[c] Theoretical data from Ref. 27, which reports also similar values by using normconserving pseudopotentials or the LDA approximation.

[d] Experimental data from Ref. 28.

[e] E_{coh} was derived from $\Delta_f H^o$ values at 0 K from Ref. 29.

[f] Experimental data from Ref. 30.

[g] Experimental data from Ref. 31.

TABLE II. Interlayer relaxations of the outermost layers for Zr- and B-terminated (2x2)-ZrB_2 (0001) surfaces.

Termination	Interlayer relaxation (%) [a]	Number of layers 4	5	10	11
Zr	Δd_{12}	-3.65	-4.18 (-4.85) [c]	-4.67	-4.49 (-5.10) [b]
	Δd_{23}	1.25	0.42 (0.71)	0.33	0.38 (0.51)
	Δd_{34}		-0.16	0.34	0.31 (0.02)
	Δd_{45}			0.39	0.43 (-0.10)
	Δd_{56}			-0.07	-0.12 (-0.03)
	Δd_{67}				
B	Δd_{12}	-6.69	-7.83 (-8.68) [c]	-7.19	-7.21 (-8.02)
	Δd_{23}	1.98	2.54 (2.31)	2.15	2.19 (1.83)
	Δd_{34}		0.70	0.35	0.27 (0.10)
	Δd_{45}			-0.31	-0.06 (-0.42)
	Δd_{56}			-0.40	-0.25 (-0.60)

[a] Defined as $\Delta d_{ij} = \left(\frac{d_{ij}(\text{slab}) - d_{ij}(\text{bulk})}{d_{ij}(\text{bulk})} \right) \times 100 \ (\%)$

[b] Theoretical data from Ref. 35 using an (1x1) unit cell.

[c] Theoretical data from Ref. 36 using an (1x1) unit cell.

TABLE III. Calculated GGA-PBE adsorption energies and geometries for one oxygen atom over the ZrB_2 (0001) surface, with a four-layer slab model (relaxing the first two layers) and a (2 × 2) supercell on different sites for both face Zr- and B-terminations

Site	E_{ad} (eV) [a]	d(O-Zr) (Å) [b]	d(O-B) (Å) [b]	Δz (Å) [c]	z(O)(Å) [d]	ν (cm^{-1}) [e]		
						⊥	∥	
				Zr-terminated				
H1	8.53	2.129	2.984	0.077	1.162	462.8	348.5	348.2
B1	7.96	2.042	3.238	0.065	1.321	521.3	467.8	173.1i
T1	5.88	1.886	4.115	0.098	1.886	700.8	158.4i	155.8i
				B-terminated				
B2	6.30	3.311	1.441	0.144	1.082	706.1	499.8	246.0
M2	5.28	3.128	1.375	0.108	1.076	762.3	263.7	308.6i
T2	4.97	3.567	1.319	0.098	1.319	864.7	150.3i	191.1i
H2	2.96	2.443	2.043	0.031	0.759	376.1	424.4i	425.4i

[a] The atomic coverage is 1/8 (12.5%) or 1/12 (8.3%) considering only the available most stable sites (i.e., H1 and B2) for Zr- or B-terminations, respectively.
[b] The shortest O-Zr and O-B distances for each site and surface termination are shown.
[c] Vertical z shift of the closest surface atoms to O adatom with respect the clean slab geometry.
[d] The z coordinate of O adatom, taking z = 0 at the closest surface atoms.
[e] Harmonic vibrational frequencies of the atomic adsorbate with respect to the rigid substrate, approximately classified as perpendicular and parallel modes.

TABLE IV. Calculated GGA-PBE adsorption energies and geometries for two oxygen atoms over the ZrB_2 (0001) surface, with a four-layer slab model (relaxing the first two layers) and a (2 × 2) supercell on different sites for both face Zr- and B-terminations.

Sites	E_{ad} (eV) [a]	d(O-Zr) (Å) [b]	d(O-B) (Å) [b]	d(O-O) (Å)	Δz (Å) [c]	z(O)(Å) [d]	ν (cm^{-1}) [e] ⊥	ν (cm^{-1}) [e] ∥	ν (cm^{-1}) [e] ∥
				Zr-terminated					
H1 + H1(A)	7.83	1.981, 1.981	3.054, 3.054	2.461	0.135	1.161, 1.161	663.1 561.6	395.2 239.5	193.9 106.8
H1 + H1(B)	8.37	2.086, 2.087	2.977, 2.977	3.179	0.115	1.114, 1.114	481.7 467.6	378.8 341.8	327.1 319.2
H1 + H1(C)	8.45	2.112, 2.112	2.973, 2.973	3.671	0.164	1.045, 1.045	454.3 438.0	414.0 413.7	378.5 378.1
				B-terminated					
B2 + B2(A)	6.45	3.456, 3.458	1.379, 1.379	2.305	0.986	0.399, 0.401	891.5 725.2	584.7 538.9	378.8 233.5
B2 + B2(B)	6.19	3.243, 3.315	1.396,1.412	2.751	0.363	0.740, 0.853	737.1 704.4	559.6 540.6	284.8 247.3
B2 + B2(C)	6.09	3.322, 3.322	1.433, 1.433	3.179	0.182	1.024, 1.023	688.9 654.5	571.1 539.5	270.7 206.7
B2 + B2(D)	6.23	3.299, 3.300	1.439, 1.439	3.179	0.121	1.096, 1.095	725.6 708.5	553.4 503.0	248.1 240.5

[a] Adsorption energy per O atom. The atomic coverage is 2/8 (25.0%) or 2/12 (16.7%) considering only the available most stable sites (i.e., H1 and B2) for Zr- or B-terminations, respectively. Values for both O adatoms (e.g., H1 and H1(A)) are given separated by a comma.
[b] The shortest O-Zr and O-B distances for each site and surface termination are shown.
[c] Vertical z shift of the closest surface atoms to O adatom with respect the clean slab geometry.
[d] The z coordinate of O adatom, taking z = 0 at the closest surface atoms.
[e] Harmonic vibrational frequencies of the atomic adsorbates with respect to the rigid substrate, approximately classified as perpendicular and parallel modes.

TABLE V. Calculated GGA-PBE energies and geometries for O_2 interaction over the ZrB_2 (0001) surface, with a four-layer slab model (relaxing the first two layers) and a (2 × 2) supercell on the B-terminated face.

Sites	E (eV) [a]	d(B-B) (Å)	d(O-B) (Å)	d(O-O) (Å)	ν (cm^{-1})[b]		
					⊥	‖	
MIN1	2.63	1.926	1.492, 1.492	1.436	648.4 576.8	841.1 269.9	292.7 97.0
TS1	0.39	1.856	3.188, 3.188	1.237	1505.6 71.6i	63.1 56.3	28.3 26.1
TS2	0.27	1.943	1.446, 1.446	1.680	642.3 635.3	246.5 87.6	152.5 639.3i

[a] Adsorption energy (E_{ad}) for the minimum and energy barriers ($\Delta V^{\neq}$) respect to the closest minimum for both transition states.
[b] Harmonic vibrational frequencies of the atomic adsorbates with respect to the rigid substrate, approximately classified as perpendicular and parallel modes.

TABLE VI. Calculated GGA-PBE energies and geometries for Eley-Rideal reaction over the ZrB_2 (0001) surface, with a four-layer slab model (relaxing the first two layers) and a (2 × 2) supercell on the B-terminated face.

Sites	E (eV) [a]	d(B-B) (Å)	d(O-B) (Å)	d(O-O) (Å)	ν (cm^{-1})[b]		
					⊥	‖	
MIN2	0.60	2.029	1.493, 1.493	1.366	941.4 373.2	633.4 213.5	176.5 75.1
TS3	0.51	1.963	2.244, 2.246	1.255	1331.2 137.2i	285.4i 54.3	201.3 130.1

[a] Adsorption energy (E_{ad}) for the minimum and energy barrier ($\Delta V^{\neq}$) respect to $O_{(g)} + O_{(ad)}$.
[b] Harmonic vibrational frequencies of the atomic adsorbates with respect to the rigid substrate, approximately classified as perpendicular and parallel modes.